

Article

Characterization of Metabolic Correlations of Ursodeoxycholic Acid with Other Bile Acid Species through In Vitro Sequential Metabolism and Isomer-Focused Identification

Wei Li ¹, Wei Chen ¹, Xiaoya Niu ¹, Chen Zhao ², Pengfei Tu ¹, Jun Li ¹ , Wenjing Liu ^{3,*} and Yuelin Song ^{1,*} 

¹ Modern Research Center for Traditional Chinese Medicine, Beijing Research Institute of Chinese Medicine, Beijing University of Chinese Medicine, Beijing 100029, China; lw160221071@163.com (W.L.)

² Zhangzhou Pien Tze Huang Pharmaceutical Co., Ltd., Zhangzhou 363000, China

³ School of Pharmacy, Henan University of Chinese Medicine, Zhengzhou 450046, China

* Correspondence: liuwj107@163.com (W.L.); syltwc2005@163.com (Y.S.)

Abstract: As a first-line agent for cholestasis treatment in a clinic, ursodeoxycholic acid rectifies the perturbed bile acids (BAs) submetabolome in a holistic manner. Considering the endogenous distribution of ursodeoxycholic acid and extensive occurrences of isomeric metabolites, it is challenging to point out whether a given bile acid species is impacted by ursodeoxycholic acid in a direct or indirect manner, thus hindering the therapeutic mechanism clarification. Here, an in-depth exploration of the metabolism pattern of ursodeoxycholic acid was attempted. Sequential metabolism in vitro with enzyme-enriched liver microsomes was implemented to simulate the step-wise metabolism and to capture the metabolically labile intermediates in the absence of endogenous BAs. Squared energy-resolved mass spectrometry (ER²-MS) was utilized to achieve isomeric identification of the conjugated metabolites. As a result, 20 metabolites (M1–M20) in total were observed and confirmatively identified. Of those, eight metabolites were generated by hydroxylation, oxidation, and epimerization, which were further metabolized to nine glucuronides and three sulfates by uridine diphosphate-glycosyltransferases and sulfotransferases, respectively. Regarding a given phase II metabolite, the conjugation sites were correlated with first-generation breakdown graphs corresponding to the linkage fission mediated by collision-induced dissociation, and the structural nuclei were identified by matching second-generation breakdown graphs with the known structures. Together, except for intestinal-bacteria-involved biotransformation, the current study characterized BA species directly influenced by ursodeoxycholic acid administration. Moreover, sequential metabolism in vitro should be a meaningful way of characterizing the metabolic pathways of endogenous substances, and squared energy-resolved mass spectrometry is a legitimate tool for structurally identifying phase II metabolites.

Keywords: ursodeoxycholic acid; metabolites; isomeric identification; conjugation site; squared energy-resolved mass spectrometry



Citation: Li, W.; Chen, W.; Niu, X.; Zhao, C.; Tu, P.; Li, J.; Liu, W.; Song, Y. Characterization of Metabolic Correlations of Ursodeoxycholic Acid with Other Bile Acid Species through In Vitro Sequential Metabolism and Isomer-Focused Identification. *Molecules* **2023**, *28*, 4801. <https://doi.org/10.3390/molecules28124801>

Academic Editor: Petr Bednar

Received: 29 May 2023

Revised: 10 June 2023

Accepted: 13 June 2023

Published: 16 June 2023



Copyright: © 2023 by the authors. Licensee MDPI, Basel, Switzerland. This article is an open access article distributed under the terms and conditions of the Creative Commons Attribution (CC BY) license (<https://creativecommons.org/licenses/by/4.0/>).

1. Introduction

Bile acids (BAs) are derivatives of hepatic cholesterol metabolites, which play a key role in nutrient absorption and the biliary secretion of lipids, toxic metabolites, and xenobiotics [1–4]. They also serve as significant regulators in mediating numerous physiological and pathophysiological processes through activating some nuclear receptors, such as farnesoid X receptor (FXR), pregnane X receptor (PXR), and Takeda G-protein-coupled receptor 5 (TGR5). These nuclear receptors function in the transcriptional regulation of genes involved in bile acid synthesis, transport, and metabolism [5–7]. The diversity and composition of the bile acid pool are related to their roles in diseases. Primary BAs are synthesized by the liver via a series of enzymatic reactions from cholesterol and then released into the small intestine. Furthermore, the gut microbiota is also reported to enrich

the diversity of the second BAs structures through four pathways: deconjugation of glycine or taurine, dehydrogenation, dehydroxylation, and epimerization [8–11]. Recently, some novel amino-acid-conjugated BAs, other than nor-DCA, tetra-BAs, 3,7,12,24-tetrol-26,27-dinorcholetane-24-sulfate, have been mined in gut microbiota metabolism, which further enrich the diversity and composition of the BA pool [12–14]. Regarding the free BAs, oxidation frequently occurs at C-3, C-6, C-7, and C-12 sites. For conjugated BAs, tauro and glycol substitutions always occur for the C-24 carboxy group. However, the identification of BAs isomers remains a challenge.

Ursodeoxycholic acid (UDCA) is a free type of bile acid, which has been utilized for medical purposes for many years [15]. While it is considered a secondary bile acid in humans, UDCA is a primary acid derived from the host in other animal species, such as bears and mice [16]. It has been widely applied in clinical treatment for various liver disorders, such as primary biliary cholangitis (PBC) [17] and intrahepatic cholestasis [18], as well as others. Very recently, a study has shown that UDCA may have pharmacological effects against COVID-19 by reducing ACE2 levels and SARS-CoV-2 infection [19]. Nevertheless, the effects of UDCA on the enterohepatic circulation of BAs have yet to be fully investigated. The bile acid pool plays a critical role in reflecting the physiological or pathological status of an organism, especially the liver, together with intestine organs where most bile acid metabolism occurs. To address this gap, we conducted a sequential metabolism of UDCA *in vitro* and clarified how these metabolic processes occur *in vivo* with other BAs. This research may help us better understand the effects of UDCA administration on the enterohepatic circulation of BAs and provide insight into its potential therapeutic application.

With the rapid advancement of the MS/MS technique, it is currently favored as a cutting-edge tool for metabolites' characterization owing to its superior sensitivity, as well as the unique advantage of generating rich structural information, primarily in terms of high-resolution (HR) mass-to-charge ratio (m/z). The online energy-resolved MS (online ER-MS) could provide the molecular descriptors, such as CE_{50} values and optimal collision energy (OCE), to determine the conjugated sites [20]. Recently, multiple-dimension MS analysis has become more and more popular, particularly in natural product structure identification at home and abroad. For instance, Qtrap-MS is a hybrid mass spectrometer, which combines the features of triple-quadrupole (QQQ) and ion trap (IT) instruments. It is composed of a quadrupole cell and a linear ion trap (LIT) chamber, which offers superior sensitivity and selectivity for targeted metabolomics analysis. Undoubtedly, it serves as the best choice for performing two consecutive online ER-MS assays, known as ER²-MS, which provide more detailed substructural information about the metabolites being analyzed. Compared with multiple-reaction monitoring (MRM) corresponding to the first ER-MS measurement [21], the MRM cubed (MRM³) algorithm exhibits suitable characteristics for meeting the second ER-MS assay requirement. The MRM³ algorithm allows the selection of specific fragmentation patterns and detection of diagnostic ions based on their unique structural characteristics. This approach improves the specificity and selectivity of the analysis and enables the identification of metabolites with greater accuracy. For instance, for BA glucuronides, the glucuronidation position can be identified by applying the first online ER-MS program to $[M-H]^- > [M-H-C_6H_8O_6]^-$ because a molecular descriptor, namely OCE, is tightly correlated with the glucuronidation site. Subsequently, $[M-H]^- > [M-H-C_6H_8O_6]^- > [M-H-C_6H_8O_6]^-$ participates in the MRM³ assay, and the second ER-MS measurement is accomplished by assigning progressive AF2 values to a panel of comparable MS³ experiments. As a result, BA glucuronides could be identified through ER²-MS.

Here, we conducted an experiment to investigate the sequential metabolism of UDCA *in vitro* and identify its transformation metabolites using liver microsomes from humans and mice, which are enriched with fruitful phase I and II metabolic enzymes. UDCA-*d*₄ was performed to validate the metabolic products of UDCA. Subsequently, the confidential metabolic structures were identified through ER²-MS, including OCE and AF2 values

molecular descriptors. To detect trace metabolites, the routine analytical pipeline Qtrap-MS with *p*MRM acquisition mode was performed subsequently and captured the diagnostic fragmentation ions. Herein, an integrated workflow (Figure 1) was proposed to eliminate the process of the experiment. Additionally, Q Exactive-MS was utilized to acquire the high-resolution MS/MS information. The findings acquired in this study will assist in enhancing our comprehension of the biotransformation bonds associated with other bile acids, not merely UDCA. Furthermore, ER²-MS enabled us to obtain an analytical pathway to enhance the potential for identifying isomers via LC-MS.

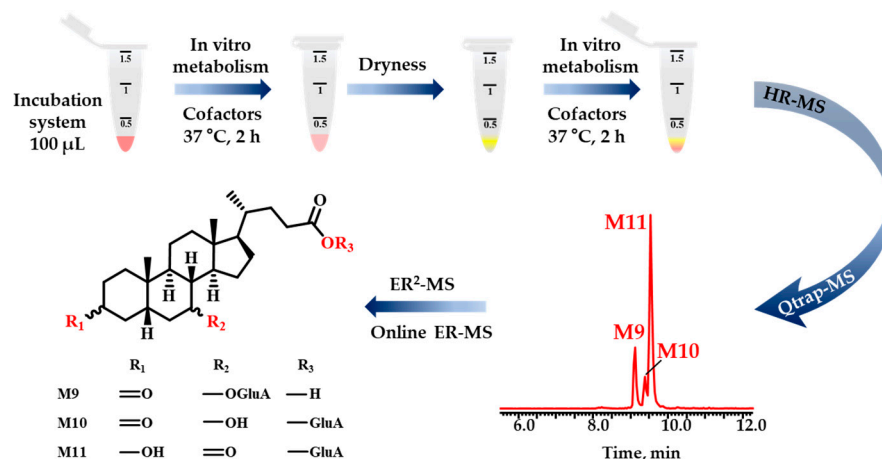


Figure 1. The workflow comprising three primary steps was proposed. Firstly, UDCA underwent sequential metabolism *in vitro* in a NADPH incubation system. The phase I metabolic products served as substrates for phase II metabolism after being evaporated to dryness with nitrogen. Secondly, the structural characterization of metabolites, even the minor ones, was accomplished by combining HR-MS with Qtrap-MS. Thirdly, the ER²-MS strategy was employed for structural identification of those isomers.

2. Results and Discussion

2.1. Identification of *In Vitro* Sequential Metabolites of UDCA

In vitro sequential metabolism of UDCA could provide an insight into the transformation of bile acids into each other, particularly in a case where UDCA was administered. In some way, this process may also occur naturally and the real condition could be performed *in vivo*. In total, 20 metabolites were tentatively identified by high-resolution MS combined with the ER²-MS strategy (Table S1).

LC-MS/MS behaviors of BAs. The mass fragmentation rules were clearly summarized in the literature [22–24] as follows. Unconjugated BAs were derived from cholic acid (CA) or CDCA via various biosynthetic pathways. Free BAs mainly participated in phase I metabolism of UDCA, which included oxidation, epimerization, and hydroxylation. It is always observed that dehydroxylation and decarboxylation on the sterol backbone result in neutral losses of H₂O (18 Da), CO (28 Da), and CO₂ (44 Da). Conjugated BAs are formed through the glycine and taurine modification of the terminal carboxyl group of free BAs. Additionally, the sulfated and glucuronidated groups occur in the hydroxyl group sites of BAs corresponding to characteristic neutral losses of SO₃ (80.06 Da) and glucuronic acid (176.12 Da). Furthermore, our group established an in-house database containing 201 BAs, which was subsequently employed to characterize metabolites according to all the aforementioned rules.

Structural characterization of UDCA metabolites using LC-MS/MS information. For UDCA phase I metabolites, there were eight metabolites identified as M1–M8 (Table S1), namely 7 β -hydroxy-3-oxo-5 β -cholan-24-oic acid (M1), 7-ketolithocholic acid (M2), CDCA (M3), 3 β ,7 α -dihydroxy-6-oxo-5 β -cholan-24-oic acid or 3 β ,6 α -dihydroxy-7-oxo-5 β -cholan-24-oic acid (M4), 3 α ,7 β -dihydroxy-12-oxo-5 β -cholan-24-oic acid (M5), 3 β ,7 β ,12 α -trihydroxy-5 β -cholan-24-oic acid (M6), ursocholic acid (M7), and β -MCA (M8). After the NADPH

regeneration system, all samples were concentrated to dryness with nitrogen gas. Then, the residues of phase I products served as phase II substrates to carry out the reaction. For UDCA phase II metabolites, there were only three metabolites identified as **M13**, **M15**, and **M19**, including UDCA-3-*O*-glucuronide (**M13**), β -MCA-3-*O*-glucuronide (**M15**), and UDCA-3-sulfate (**M19**) (Table S1).

M1 and **M2** were taken as cases to clarify the structural annotation of metabolites, which shared an identical $[M - H]^-$ ion at m/z 389.2702, and the elemental composition was calculated as $C_{24}H_{38}O_4$. In comparison to prototype UDCA, oxidation should be responsible for reducing two hydrogen atoms. When Q1 ions entered the collision chamber to perform collision-induced dissociation, the primary fragment ions were observed as m/z 371.2637 ($C_{24}H_{35}O_3^-$), m/z 343.2656 ($C_{23}H_{35}O_2^-$), m/z 325.2553 ($C_{23}H_{33}O^-$), and m/z 69.0346 ($C_4H_6O^-$). These ions mainly orientated from neutral cleavages of H_2O , $HCOOH$, and ring-A from C1-C10 to C4-C5. Among them, only **M1** occurred with m/z 69.0346, which indicated the dehydrogenation of the C3-OH group. Therefore, **M1** was identified as the C3-OH oxidation of UDCA, forming 7 β -hydroxy-3-oxo-5 β -cholan-24-oic acid. This conclusion was validated by the spectrum of UDCA- d_4 , in which the cleavage of ring-A from C1-C10 to C4-C5 was detected. Undoubtedly, **M2** was identified as the C7-OH group dehydrogenated metabolite, attributed to 7-ketolithocholic acid. The mass fragmentation pathways of **M1** and **M2** are proposed in Figure S1. Additionally, **M7** was identified as UCA compared to the authentic compound with retention time.

BAs mining based on *p*MRM strategy. In order to dig and clarify in depth the UDCA in vitro metabolism profiles involved in phase II reactions, the *p*MRM scan mode was carefully developed to identify the comprehensive metabolites, especially for trace metabolic products. As a result, a total of twenty metabolites were detected and tentatively characterized as **M1–M20** (Table S1) in the negative ion mode, while without UDCA being involved, HLM (Figure S2) or MLM (Figure S3) was detected with the NADPH incubation system in vitro. Additionally, glucuronidation (Figure S4A,B) or sulfation (Figure S4C,D) assays were performed without UDCA involvement in HLM or MLM detection with the UDPGA or PAPS incubation system. For the phase I reaction, the **M1–M8** metabolites are shown in Figure 2A, of which the isotope labeling metabolites were spotted correspondingly via UDCA- d_4 in vitro incubation (Figure S5A). In terms of phase II metabolism containing glucuronidation and sulfonation, the compounds comprising carboxy groups or phenolic hydroxyl groups tend to combine with glucuronic acid or sulfate. Hence, there were nine glucuronide products shown in Figure 2B (**M9–M17**), including 7 β -hydroxy-3-oxo-5 β -cholan-24-oic acid-7-*O*-glucuronide (**M9**), 7 β -hydroxy-3-oxo-5 β -cholan-24-oic acid-24-*O*-glucuronide (**M10**), 7-ketolithocholic acid-24-*O*-glucuronide (**M11**), UDCA-7-*O*-glucuronide (**M12**), UDCA-3-*O*-glucuronide (**M13**), UCA-7-*O*-glucuronide (**M14**), β -MCA-3-*O*-glucuronide (**M15**), UCA-3-*O*-glucuronide (**M16**), 3 β ,7 β ,12 α -trihydroxy-5 β -cholan-24-oic acid-3-*O*-glucuronide (**M17**). Then, three sulfated metabolites were observed (Figure 2B)—a panel of bile acids whose hydroxy groups were modified through the sulfuric acid—yielded from the NADPH reaction system, including 7 β -hydroxy-3-oxo-5 β -cholan-24-oic acid-7-sulfate (**M18**), UDCA-3-sulfate (**M19**), and UDCA-7-sulfate (**M20**). Among them, **M2**, **M3**, **M7**, and **M8** were confidentially identified by authentic compounds with retention time and mass fragment information. However, a group of isomers, **M14** ($t_R = 7.78$ min), **M15** ($t_R = 8.44$ min), **M16** ($t_R = 8.62$ min), and **M17** ($t_R = 9.2$ min), were captured by m/z 583.31 > 407.28 with the *p*MRM program (Figure 3A). Only **M15** was hunted by HR-MS and observed primary MS^1 at m/z 583.3144 ($[M - H]^-$) and fragment ions, including 407.2813, 175.0255, and 113.0250 (Figure 3B), corresponding to $C_{24}H_{39}O_5^-$, $C_6H_7O_6^-$, and $C_5H_5O_3^-$. Therefore, **M15** was tentatively characterized as the 3 β ,7 β ,12 α -trihydroxy-5 β -cholan-24-oic acid-glucuronide, UCA-glucuronide, or β -MCA-glucuronide combined with those well-defined mass cracking rules and phase I metabolism. **M12** and **M13** were identified as UDCA-glucuronide or CDCA-glucuronide. Similarly, **M9**, **M10**, and **M11** were identified as 7 β -hydroxy-3-oxo-5 β -cholan-24-oic acid-glucuronide or 7-ketolithocholic acid-glucuronide. **M18** and **M20** were determined as

7 β -hydroxy-3-oxo-5 β -cholan-24-oic acid-sulfate and UDCA-sulfate. **M19** was characterized as UDCA-3-sulfate through the incubation of UDCA with human recombinase SULT2A1 in our laboratory. For phase II metabolites, the isotope labeling metabolites were also detected correspondingly via UDCA- d_4 in vitro incubation (Figure S5B), except for **M19**. In order to solve the characterization of isomeric metabolites, we further established a strategy based on ER²-MS for in-depth confirmation of the sites of those conjugated metabolites.

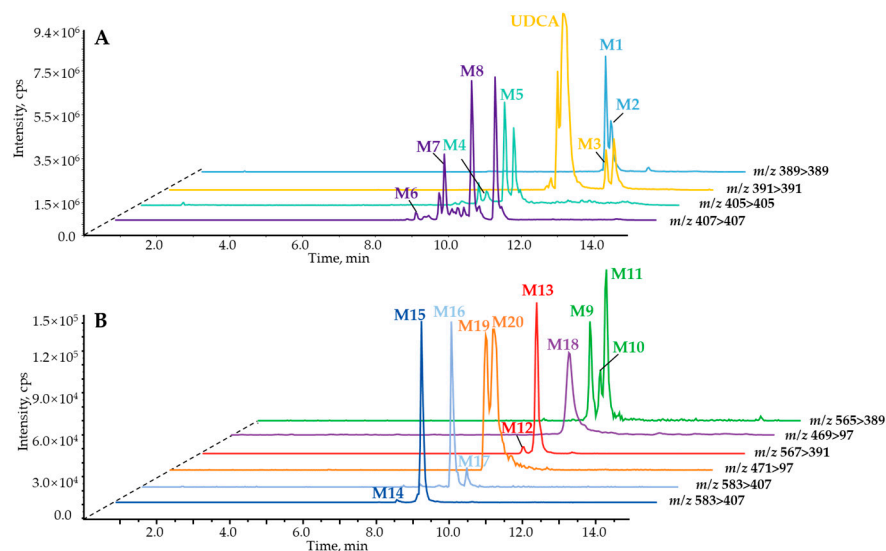


Figure 2. Extracted ion current chromatogram of phase I metabolites (A), phase II glucuronidated and sulfated metabolites (B) of UDCA from LC-pMRM program.

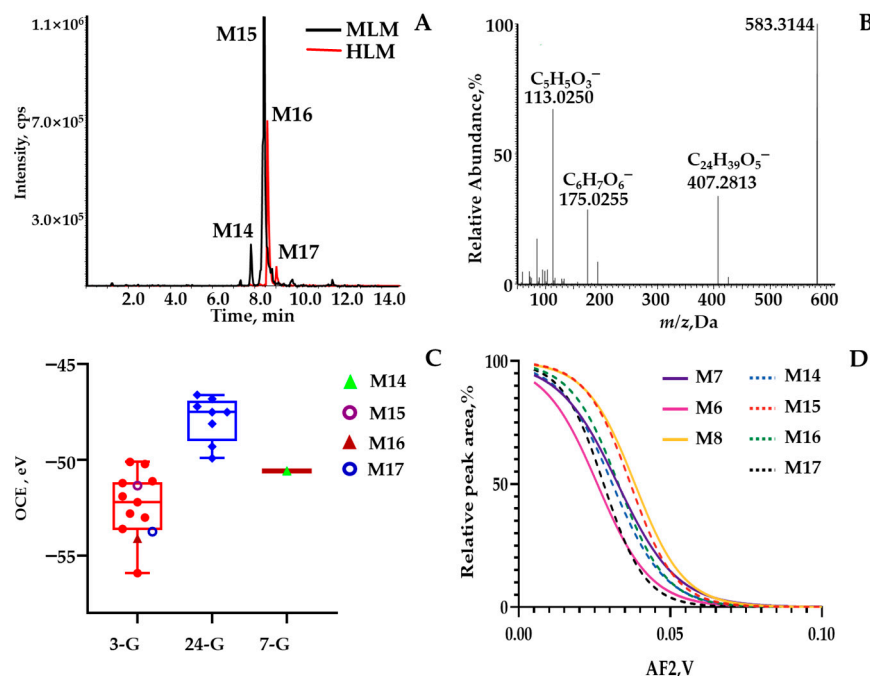


Figure 3. (A) Extracted ion current chromatogram (m/z 583.3 > 407.3) from LC-pMRM program; (B) MS² spectrum of the quasimolecular ion ($[M - H]^-$) of **M15** acquired by LC-MS; (C) Box plot for the OCE scattering pattern of m/z 583.3 > 407.3 against different glucuronidation sites (C-3, C-7, or C-24) via assaying literature in our group; (D) Overlaid sigmoid-shaped second-generation breakdown graphs (relative intensity of 50% against AF2 values) acquired by programming m/z 583.3 > 407.3 > 407.3 for **M6**–**M8** and **M14**–**M17**.

2.2. Phase II Metabolites' Identification by ER²-MS

Although the MS analysis provided the information on the free and conjugated type BAs, the accurate characterization of UDCA phase II metabolites containing isomers remains challenging. In our group, extensive efforts were made to strengthen the structural annotation evidence via ER²-MS measurements, which were established to achieve as many as 201 BAs [25]. Herein, we proposed an *p*MRM interpretation strategy in an ER²-MS manner, which mainly aims to synergistically screen the conjugated sites and substructures of all phase II metabolites.

Identity metabolites' consolidation via application of ER²-MS. The first ER-MS strategy was used to assign the glucuronide-conjugated site and the sulfate-conjugated site. Second-generation breakdown graphs were employed to confirm the scaffold, which was featured by the configuration and the location of carbonyl and/or hydroxy groups. **M15** was employed as a representative case. After undergoing the first ER-MS assay, OCE corresponding to m/z 583.3 > 407.3 was calculated to be -51.33 eV from a Gaussian-shaped first-generation breakdown graph (Figure 3C), located exactly within the OCE window 3-G rather than the ranges derived from 7-G and 24-G. The OCE distribution diagram was rendered through assaying authentic compounds in our group [25]. Consequently, glucuronide occurred for C3-OH. Following the second ER-MS assay, a sigmoid-shaped second-generation breakdown graph resulting from m/z 583.3 > 407.3 > 407.3 matched well with the one generated by applying m/z 407.3 > 407.3 > 407.3 to β -MCA (**M8**), one of the UDCA phase I metabolites (Figure 3D). However, **M14**, **M16**, and **M17** were captured as an isomer set through predefined ion transition by 583.3 > 407.3 simultaneously. The OCE corresponding to m/z 583.3 > 407.3 for **M15** isomers were calculated to be -50.57 eV, -53.74 eV, and -54.11 eV, respectively, from the first breakdown graph, located exactly within the OCE window 3-G. According to the UDCA phase I metabolites for m/z 407.3 > 407.3, there were only two hydroxyl sites conjugated with glucuronide, except for **M15**. Following the second ER-MS assay, a sigmoid-shaped second-generation breakdown graph resulting from m/z 583.3 > 407.3 > 407.3 to **M14**, **M16**, and **M17** matched well with the phase I metabolites generated by applying m/z 407.3 > 407.3 > 407.3 to **M7** and **M6**. As a result, **M14**, **M16**, and **M17** were tentatively identified as UCA-7-O-glucuronide, UCA-3-O-glucuronide, and $3\beta,7\beta,12\alpha$ -trihydroxy-5 β -cholan-24-oic acid-3-O-glucuronide.

M9, **M10**, and **M11** were captured as an isomeric set through predefined ion transitions as m/z 565.3 > 389.3 at 9.16 min, 9.37 min, and 9.52 min. They were predefined as the glucuronide-conjugated metabolites from **M1** or **M2** after phase I bioconversion. Then, great efforts were made to confirm the glucuronide-conjugated site, namely C3-OH, C7-OH, or C24-COOH. The following OCEs of the diagnostic ion at m/z 389.3 were calculated to be -47.68 eV, -48.38 eV, and -49.74 eV for the first breakdown graph. Then, we observed the OCEs of these isomers located exactly within the OCE window 7-G and 24-G (Figure 4A). In depth, the scaffolds of **M9**, **M10**, and **M11** were confirmatively configured as **M1** and **M2** (Figure 4B). Therefore, the structures of **M9**, **M10**, and **M11** were respectively identified as 7β -hydroxy-3-oxo-5 β -cholan-24-oic acid-7-O-glucuronide, 7β -hydroxy-3-oxo-5 β -cholan-24-oic acid-24-O-glucuronide, and 7-ketolithocholic acid-24-O-glucuronide.

M19 and **M20** were captured through predefined ion transitions as m/z 469.3 > 97 and at 8.69 min and 8.92 min. For one of the metabolites (**M19**), its primary mass fragment ion species of $[M-H]^-$ (m/z 567.3202) was observed at m/z 471.2427, 96.9605, and 79.9576 (Table S1). After converting the m/z values to elemental compositions, **M19** and **M20** were regarded as the sulfated products of UDCA or CDCA. The structural identification workload subsequently turned to assigning the sulfate-conjugated site, namely C3-OH and C7-OH. Fortunately, UDCA-3-sulfate was incubated with recombinase SULT2A1 in our laboratory. **M19** was justified as UDCA-3-sulfate with a reference compound. Afterward, m/z 469.3 > 97 was subjected to the first ER-MS assays, and the OCE of **M20** was determined as -101.1 eV, located within the 7-S window of the OCE distribution diagram (Figure 4C). Moreover, the backbone to the second ER-MS was matched well with UDCA. As a result, the putative identity of **M20** was assigned to UDCA-7-sulfate by applying ER²-MS. Addi-

tionally, **M18** was identified as 7 β -hydroxy-3-oxo-5 β -cholan-24-oic acid-7-sulfate via the aforementioned workflow.

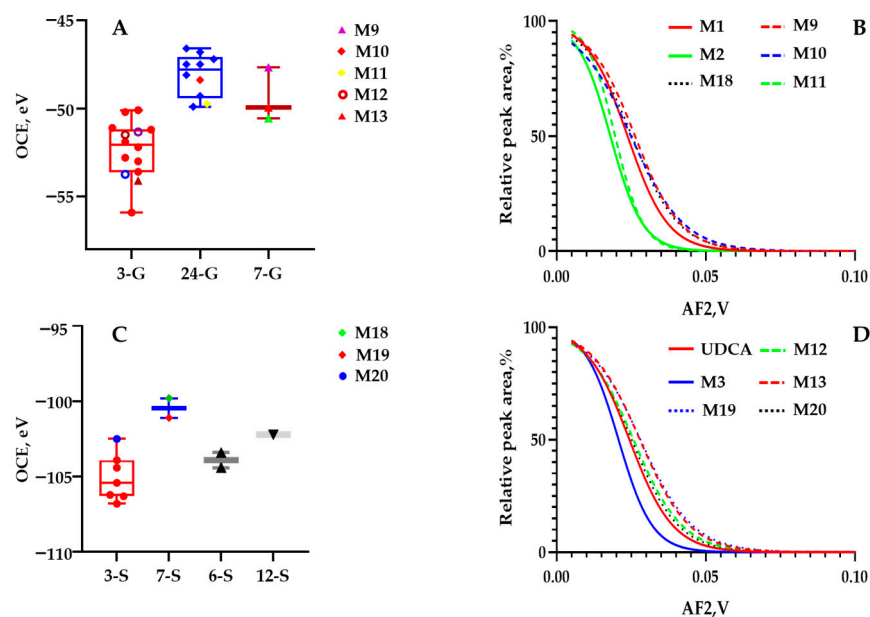


Figure 4. (A) Box plot for the OCE scattering pattern of m/z 565.3 > 389.3 and m/z 567.3 > 391.3 against different glucuronidation sites (C-3, C-7, or C-24) via assaying authentic compounds in our group; (B) Overlaid sigmoid-shaped second-generation breakdown graphs (relative intensity of 50% against AF2 values) acquired by programming m/z 389.3 > 389.3 > 389.3 for **M1** (red curve; equation: $Y = 100/(1 + 10^{((0.02379-X) \times -64.11)})$), $R^2 = 0.9862$), **M2** (green curve; equation: $Y = 100/(1 + 10^{((0.01802-X) \times -79.94)})$), $R^2 = 0.9865$), m/z 565.3 > 389.3 > 389.3 for **M9** (red dotted curve; equation: $Y = 100/(1 + 10^{((0.02630-X) \times -56.85)})$), $R^2 = 0.9864$), **M10** (blue dotted curve; equation: $Y = 100/(1 + 10^{((0.02491-X) \times -48.96)})$), $R^2 = 0.9875$), **M11** (green dotted curve; equation: $Y = 100/(1 + 10^{((0.01962-X) \times -92.44)})$), $R^2 = 0.9672$), m/z 469.3 > 97 > 97 for **M18** (black dotted curve; equation: $Y = 100/(1 + 10^{((0.01962-X) \times -92.44)})$), $R^2 = 0.9672$); (C) Box plot for the OCE scattering pattern of m/z 469.3 > 97 and m/z 471.3 > 97 against different sulfated sites (C-3, C-6, C-7, or C-12) via assaying literature in our group; (D) Overlaid sigmoid-shaped second-generation breakdown graphs (relative intensity of 50% against AF2 values) acquired by programming m/z 391.3 > 391.3 > 391.3 for **M3** (blue curve; equation: $Y = 100/(1 + 10^{((0.02077-X) \times -76.97)})$), $R^2 = 0.9630$), m/z 571.3 > 391.3 > 391.3 for **M12** (green dotted curve; equation: $Y = 100/(1 + 10^{((0.02576-X) \times -53.30)})$), $R^2 = 0.9764$), **M13** (red dotted curve; equation: $Y = 100/(1 + 10^{((0.02794-X) \times -52.25)})$), $R^2 = 0.9892$), m/z 471.3 > 97 > 97 for **M19** (blue dotted curve; equation: $Y = 100/(1 + 10^{((0.02812-X) \times -49.78)})$), $R^2 = 0.9951$), and **M20** (black dotted curve; equation: $Y = 100/(1 + 10^{((0.02516-X) \times -55.55)})$), $R^2 = 0.9391$).

M12 and **M13** were acquired as isomers through predefined ion transitions as m/z 567.3 > 391.3 at 8.83 min and 9.16 min. For one of the metabolites (**M13**), its primary mass fragment ion species of $[M-H]^-$ (m/z 567.3202) was observed at m/z 391.2863, 175.0256, 129.0200, and 113.0250 (Table S1). After converting the m/z values to elemental compositions, **M12** and **M13** were regarded as glucuronidated products of UDCA or CDCA. Then, the structural identification workload subsequently turned to assigning the glucuronide-conjugated site, namely C3-OH, C7-OH, or C24-COOH. Afterward, the OCEs of the diagnostic ion at m/z 391.3 were calculated to be -49.96 eV and -51.50 eV for **M12** and **M13** for the first breakdown graph. Then, we observed the OCEs of two isomers located exactly within the OCE window 7-G and 3-G (Figure 4A). In depth, the scaffolds of **M12** and **M13** were confirmatively confirmed as UDCA (Figure 4D). Hence, the structures of **M12** and **M13** were identified as UDCA-7-O-glucuronide and UDCA-3-O-glucuronide through application of ER²-MS with UDCA.

sulfation displayed in Figure S4, indicating a low level of conjugated bile acids in normal conditions. To confirm the products of UDCA sequential metabolism, UDCA- d_4 was incubated in parallel. As expected, biotransformed metabolites labeled with deuterium were observed in Figure S5, except for **M19**, compared to UDCA. Hitherto, great efforts have been widely made to develop methods allowing isomeric identification, from sample preparation to detection, using cutting-edge MS/MS techniques, such as ion mobility spectrometry, chemical derivatization, and energy-resolved MS [27,28]. Although a research model using in vitro cofactor-fortified liver S9 fraction was developed to compare the metabolites of CA, CDCA, LCA, and UDCA, the bile acid conjugated sites of glucuronic acid or sulfate could not be confidently confirmed [29]. Therefore, we established an approach for isomeric structural annotation in phase II metabolites based on ER²-MS, which ultimately uncovered the real identities of twelve metabolites. According to a report, CYP3A4 is the primary CYP450 enzyme responsible for metabolizing both CA and CDCA in HLM [30]. To acquire a better understanding of the metabolic network within the liver, it would be helpful to assess the related isoform of UGTs or SULTs in UDCA hepatic metabolism processes. Moreover, our findings suggest that an in vitro incubation system can serve as a cost-effective alternative for obtaining bile acid glucuronide standards, which are otherwise expensive on the market.

In the current work, we developed an integrated approach via combining high-resolution MS and the *p*MRM strategy of Qtrap-MS, which facilitated the comprehensive profiling and characterization of prototype compounds and metabolites of UDCA. In addition, ER²-MS offers a unique dimension to aid in the annotation of isomeric structures. The results showed that the biotransformation pathways of UDCA mainly included oxidation, hydrogenation, glucuronidation, and sulfonation.

3. Materials and Methods

3.1. Materials and Chemicals

Homogenized liver microsomes of humans and mice were purchased from the Research Institute for Liver Diseases Co., Ltd. (Shanghai, China). As an internal standard (IS), astragaloside IV was obtained from Yuanye Biotech Co., Ltd. (Shanghai, China). Authentic compounds, such as 7-ketolithocholic acid, UDCA, chenodeoxycholic acid (CDCA), ursolic acid (UCA), β -muricholic acid (β -MCA), and UDCA- d_4 , were commercially supplied by Yuanye Biotech Co., Ltd. (Shanghai, China). UDCA-3-sulfate (UDCA-3-S) was previously biosynthesized by SULT2A1 in our laboratory.

LC-MS grade acetonitrile (ACN), methanol, ammonium formate, as well as formic acid were obtained from Thermo-Fisher (Pittsburgh, PA, USA). Ultrapure deionized water was prepared using an in-house Millipore Milli-Q Integral water purification system (Bedford, MA, USA). Nicotinamide adenine dinucleotide phosphate (NADPH), glucose 6-phosphate (G6P), glucose-6-phosphate dehydrogenase (G6PD), uridine 5'-diphosphate glucuronic acid (UDPGA), alamethicin, dithiothreitol (DTT), D-saccharic acid-1,4-lactone monohydrate, 3'-phosphoadenosine-5'-phosphosulfate (PAPS), magnesium chloride, tris hydrochloride (Tris HCl), phosphate-buffered saline (PBS) were purchased from Yuanye Biotech Co., Ltd. (Shanghai, China).

3.2. Liver Microsomes Incubation Condition

Liver microsomes from humans (HLM) and mice (MLM) with a protein concentration of 20 mg/mL were thawed cautiously on ice and divided into aliquots for further experiments. In order to illustrate the biotransformation process of UDCA in vivo, this study performed sequential metabolism of UDCA in two steps. Firstly, for phase I metabolism, the NADPH regeneration system was composed of magnesium chloride (100 mM), Tris HCl (50 mM), G6P (10 mM), G6PD (50 U/mL), and NADPH (40 mM). For phase II metabolism, two-phase reactions were mainly involved in conjugating the hydroxyl groups with sulfo and glucuronyl groups individually. One UDPGA-related incubation system contained Tris HCl (50 mM), magnesium chloride (100 mM), alamethicin (5 mg/mL), D-saccharic

acid 1,4-lactone (20 mM), and UDPGA (40 mM). Another PAPS-oriented incubation system consisted of PBS (pH 7.4, 50 mM), DTT (5 mM), magnesium chloride (8 mM), and PAPS (10 mM). Then, authentic BAs including UDCA at a concentration of 10 mM and UDCA- d_4 labeled standard of 10 mM were added to three regeneration systems along with 0.05 mg of hepatic microsomal protein from either human or mouse, respectively. After a preincubation period of 5 min at 37 °C, the incubation reactions were initiated by adding, respectively, the NADPH, PAPS, or UDPGA and allowed to proceed at 37 °C for 2 h. The reactions were terminated with 100 μ L ice ACN containing astragaloside IV (1 μ g/mL) at a final volume of 200 μ L. For the control group, there were no substrates or microsomes present, which could be compared to the incubation systems involving UDCA or UDCA- d_4 .

3.3. Qualitative Characterization

3.3.1. Qualitative Characterization for LC-MS/MS

The incubational samples' analysis was performed on LC-Q-Exactive-MS (Thermo-Fisher Scientific, Waltham, MA, USA). Chromatographic separations were conducted on a Waters HSS T3 Column (2.1 \times 100 mm, 1.8 μ m, Milford, MA, USA). The mobile phase consisting of 1 mM aqueous ammonium formate containing 0.1% formic acid (A) and ACN (B) was programmed in gradients, as follows: 0–10 min, 10–95% B; 10–10.1 min, 95–10% B; 15 min, 10% B; and flow rate, 0.2 mL/min. The injection volume was 4 μ L, the column oven was set at 40 °C, and the autosampler chamber was maintained at 4 °C. MS¹ full scan was operated at 70,000 FWHM resolution among m/z 50–750, and automatically triggered MS/MS acquisition was conducted at 17 500 FWHM resolution within m/z 50–750 through a top-10 data-dependent acquisition algorithm. The isolation width of the precursor ion was 1.5 Da. The collision energy (CE) was set at 30 eV, with a collision energy spread (CES) of 15 eV. Data acquisition was carried out using Xcalibur software (Version 2.1.0, Thermo-Fisher Scientific).

3.3.2. Isomeric Identification through ER²-MS Strategy

First ER-MS assay. The first ER-MS was programmed to acquire first-generation breakdown graphs for the predominant MS² spectral signals of each compound using a previously described method [25]. For instance, in the case of **M15**, a UDCA phase II metabolite, the significant MS¹ spectral signal was m/z 583.31 ([M-H][−]), with primary MS² fragment signals occurring at m/z 407.28 [M-H-C₆H₈O₆][−], 175.03 [M-H-C₂₄H₄₀O₅][−], and 113.03 [M-H-C₂₄H₄₀O₅-CH₂O₃][−]. Thereafter, three ion transitions, including m/z 583.31 > 407.28, m/z 583.31 > 175.03, and m/z 583.31 > 113.03, were programmed for the first ER-MS analysis. Subsequently, a series of pseudo-ion transitions (PITs) were derived for each ion transition. Three panel PITs were generated as m/z 583.3 > 407.301, 583.3 > 407.302, 583.3 > 407.303, etc.; m/z 583.3 > 175.031, 583.3 > 175.032, 583.3 > 175.033, etc.; m/z 583.3 > 113.031, 583.3 > 113.032, 583.3 > 113.033, etc. Each PITs set was accordingly assigned progressive CEs with a step size of 2 eV among the range of −5 ~ −61 eV, such as −5 eV, −7 eV, and so forth. The MRM parameters are listed in Table S1. The aligned PITs and CEs sets were imported into the monitoring list of MRM. Afterward, the MRM responses of all PITs were normalized within the ion transition candidates and then input into GraphPad Prism 8.0 software (San Diego, CA, USA) to plot the breakdown graph for each ion transition via Gaussian fitting. The OCE corresponded to the acme of the breakdown graph.

Second ER-MS measurement. The second ER-MS assay was conducted using the MRM³ program for annotating the structures of glucuronyl-conjugated BAs in this research. Fixed CE values were assigned on the Q2 cell, while progressive AF2 values were implemented for the LIT chamber, which produced second-generation breakdown graphs through programming a sequence of MS³ experiments after constructing Q1 > Q3 > Q_{LIT} ion transitions. As an illustration, **M14**, **M15**, **M16**, and **M17** were chosen as representatives of isomeric-free BAs. For either Q1 or Q3, m/z 407.3 was defined with a fixed CE of −20 eV for the Q2 cell. Fourteen MRM³ experiments were performed with progressive AF2 values

(step size of 0.005 V), ramping up from 0.025 to 0.11 V, and m/z 407.3 with a 2 Da width was applied for each experiment. The other parameter settings followed those described in the literature [25]. The peaks of each analyte harvested from different AF2 levels were merged, normalized, and used to draw Gaussian-shaped breakdown graphs for sub-product ions with GraphPad Prism 8.0 software (San Diego, CA, USA) following the MRM³ assays.

The predictive multiple-reaction monitoring (*p*MRM) scan mode was utilized to screen for a wide range of BAs, which was accomplished by using a monitoring list previously constructed based on LC-Qtrap-MS. $[M-H]^- > [M-H]^-$ ion species were selected for hydroxylation, oxidation, and epimerization products. The precursor ion transitions of glucuronide-conjugated BAs were set to $[M-H]^-$ with the corresponding Q3 ions set at a neutral loss of glucuronyl residue ($[M-H-176.02]^-$), 175.02 Da, and 113.02 Da, whereas $[M-H]^- > [M-H-sulfonyl\ residue]^-$ and $[M-H]^- > m/z$ 96.96 Da (HSO_4^-) were set to capture the sulfation products. Ultimately, the *p*MRM program was configured to perform qualitative analysis simultaneously involving all sequential metabolites. The LC elution program was the same as high-resolution MS.

4. Conclusions

Although UDCA serves as the primary drug for cholestasis treatment, its metabolism to other bile acid species has not been fully revealed using LC-MS/MS due to its inability to address the blind drawback of isomeric metabolites. To overcome this limitation, we proposed a new strategy named ER²-MS to structurally characterize the conjugated metabolites. This was achieved by applying well-defined mass cracking rules and authentic compounds for phase I metabolites. In terms of the given phase II metabolites, the conjugation sites were correlated with first-generation breakdown graphs corresponding to the linkage fission mediated by collision-induced dissociation, and the structural nuclei were identified by matching second-generation breakdown graphs with the known structures. In this study, we used ER²-MS to detect and identify twenty metabolites (**M1–M20**), including eight phase I metabolites and twelve phase II metabolites, after *in vitro* incubation of UDCA under different regeneration systems. Furthermore, the glucuronidation and sulfation conjugation sites of UDCA were confirmed via ER-MS, while the structural nuclei were identified by ER²-MS. More importantly, the current study can provide a legitimate analytical approach for the characterization of metabolites, particularly phase II metabolites.

Supplementary Materials: The following supporting information can be downloaded at <https://www.mdpi.com/article/10.3390/molecules28124801/s1>, Figure S1: LC-MS chromatogram and proposed fragmentation pathways of oxidative products in the negative ion mode. (A) Proposed fragmentation pathways of 7 β -hydroxy-3-oxo-5 β -cholan-24-oic acid and 7-ketolithocholic acid. (B) Proposed fragmentation pathways of 7 β -hydroxy-3-oxo-5 β -cholan-24-oic acid-*d*₄ and 7-ketolithocholic acid-*d*₄. Figure S2: Extraction chromatography of incubation system from the LC-*p*MRM program (A) without UDCA and with NADPH incubation system involved in HLM; (B) without UDCA and NADPH incubation system, with HLM. Figure S3: Extraction chromatography of incubation system from the LC-*p*MRM program (A) without UDCA and with NADPH incubation system involved in MLM; (B) without UDCA and NADPH incubation system, with MLM. Figure S4: Extraction chromatography of incubation system from the LC-*p*MRM program (A) without UDCA and with UDPGA incubation system involved in HLM or MLM; (B) without UDCA and UDPGA incubation system, with HLM or MLM; (C) without UDCA and with PAPS incubation system involved in HLM; (D) without UDCA and PAPS incubation system, with HLM or MLM. Figure S5: (A) Extracted ion current chromatogram (phase I metabolites of UDCA-*d*₄) from the LC-*p*MRM program; (B) Extracted ion current chromatogram (phase II glucuronidated and sulfated metabolites of UDCA-*d*₄) from the LC-*p*MRM program. Table S1: The chromatographic, MS/MS information, optimized ion transitions and collision energy information on UDCA *in vitro* metabolites generated from incubation of liver microsomes (human and mouse) by *p*MRM program.

Author Contributions: W.L. (Wei Li): Methodology, Investigation, Writing—Original Draft; W.C.: Visualization, Data Analysis, Writing—Original Draft; X.N.: Visualization, Data Analysis; C.Z.: Data Analysis, Writing—Original Draft; P.T.: Project Administration; J.L.: Review and Editing, Funding Acquisition; W.L. (Wenjing Liu): Writing—Review and Editing; Y.S.: Conceptualization, Writing—Review and Editing, Funding Acquisition. All authors have read and agreed to the published version of the manuscript.

Funding: This study was financially supported by the National Natural Science Foundation of China (Nos. 81973444 and 81773875).

Institutional Review Board Statement: Not applicable.

Informed Consent Statement: Not applicable.

Data Availability Statement: Not applicable.

Conflicts of Interest: The authors declare no conflict of interest.

Sample Availability: Not applicable.

References

1. Hofmann, A.F.; Hagey, L.R. Bile Acids: Chemistry, Pathochemistry, Biology, Pathobiology, and Therapeutics. *Cell Mol. Life Sci.* **2008**, *65*, 2461–2483. [[CrossRef](#)]
2. Hofmann, A.F. Bile acids: Trying to understand their chemistry and biology with the hope of helping patients. *Hepatology* **2009**, *49*, 1403–1418. [[CrossRef](#)] [[PubMed](#)]
3. de Aguiar Vallim, T.Q.; Tarling, E.J.; Edwards, P.A. Pleiotropic roles of bile acids in metabolism. *Cell Metab.* **2013**, *17*, 657–669. [[CrossRef](#)] [[PubMed](#)]
4. Hofmann, A.F.; Hagey, L.R. Key discoveries in bile acid chemistry and biology and their clinical applications: History of the last eight decades. *J. Lipid Res.* **2014**, *55*, 1553–1595. [[CrossRef](#)]
5. Kumari, A.; Pal Pathak, D.; Asthana, S. Bile acids mediated potential functional interaction between FXR and FATP5 in the regulation of lipid metabolism. *Int. J. Biol. Sci.* **2020**, *16*, 2308–2322. [[CrossRef](#)] [[PubMed](#)]
6. Watanabe, M.; Houten, S.M.; Matak, C.; Christoffolete, M.A.; Kim, B.W.; Sato, H.; Messaddeq, N.; Harney, J.W.; Ezaki, O.; Kodama, T.; et al. Bile acids induce energy expenditure by promoting intracellular thyroid hormone activation. *Nature* **2006**, *439*, 484–489. [[CrossRef](#)]
7. Thomas, C.; Pellicciari, R.; Pruzanski, M.; Auwerx, J.; Schoonjans, K. Targeting bile-acid signalling for metabolic diseases. *Nat. Rev. Drug Discov.* **2008**, *7*, 678–693. [[CrossRef](#)]
8. Ridlon, J.M.; Kang, D.J.; Hylemon, P.B.; Bajaj, J.S. Bile acids and the gut microbiome. *Curr. Opin. Gastroenterol.* **2014**, *30*, 332–338. [[CrossRef](#)]
9. Tore Midtvedt, M.D. Microbial bile acid transformation. *Am. J. Clin. Nutr.* **1974**, *27*, 1341–1347. [[CrossRef](#)]
10. Gerard, P. Metabolism of cholesterol and bile acids by the gut microbiota. *Pathogens* **2013**, *3*, 14–24. [[CrossRef](#)]
11. Begley, M.; Gahan, C.G.; Hill, C. The interaction between bacteria and bile. *FEMS Microbiol. Rev.* **2005**, *29*, 625–651. [[CrossRef](#)]
12. Zhu, Q.F.; Wang, Y.Z.; An, N.; Hao, J.D.; Mei, P.C.; Bai, Y.L.; Hu, Y.N.; Bai, P.R.; Feng, Y.Q. Alternating dual-collision energy scanning mass spectrometry approach: Discovery of novel microbial bile-acid conjugates. *Anal. Chem.* **2022**, *94*, 2655–2664. [[CrossRef](#)] [[PubMed](#)]
13. Wang, Y.Z.; Mei, P.C.; Bai, P.R.; An, N.; He, J.G.; Wang, J.; Zhu, Q.F.; Feng, Y.Q. A strategy for screening and identification of new amino acid-conjugated bile acids with high coverage by liquid chromatography-mass spectrometry. *Anal. Chim. Acta* **2023**, *1239*, 340691. [[CrossRef](#)] [[PubMed](#)]
14. Zhang, Y.; Huang, Y.; Fan, J.; Zhang, M.; Hasan, A.; Yi, Y.; Yu, R.; Zhou, X.; Ye, M.; Qiao, X. Expanding the scope of targeted metabolomics by one-pot microscale synthesis and tailored metabolite profiling: Investigation of bile acid–amino acid conjugates. *Anal. Chem.* **2022**, *94*, 16596–16603. [[CrossRef](#)] [[PubMed](#)]
15. Wang, D.Q.; Carey, M.C. Therapeutic uses of animal biles in traditional Chinese medicine: An ethnopharmacological, biophysical chemical and medicinal review. *World J. Gastroenterol.* **2014**, *20*, 9952–9975. [[CrossRef](#)]
16. Hagey, L.R.; Crombie, D.L.; Espinosa, E.; Carey, M.C.; Igimi, H.; Hofmann, A.F. Ursodeoxycholic acid in the Ursidae: Biliary bile acids of bears, pandas, and related carnivores. *J. Lipid Res.* **1993**, *34*, 1911–1917. [[CrossRef](#)]
17. Xuan, G.Y.; Ding, D.W.; Liu, N.; Hu, Y.N.; Yang, F.F.; Tian, S.Y.; Sun, H.; Yang, J.Q.; Xu, A.; Guo, G.Y.; et al. Efficacy and safety of fenofibrate add-on therapy in patients with primary biliary cholangitis refractory to ursodeoxycholic acid: A retrospective study and updated meta-analysis. *Front. Pharmacol.* **2022**, *13*, 948362.
18. Ovadia, C.; Perdones-Montero, A.; Fan, H.M.; Mullish, B.H.; McDonald, J.A.K.; Papacleovoulou, G.; Wahlström, A.; Ståhlman, M.; Tsakmaki, A.; Clarke, L.C.D.; et al. Ursodeoxycholic acid enriches intestinal bile salt hydrolase-expressing Bacteroidetes in cholestatic pregnancy. *Sci. Rep.* **2020**, *10*, 3895. [[CrossRef](#)]
19. Brevini, T.; Maes, M.; Webb, G.J.; John, B.V.; Fuchs, C.D.; Buescher, G.; Wang, L.; Griffiths, C.; Brown, M.L., 3rd; Scott, W.E.; et al. FXR inhibition may protect from SARS-CoV-2 infection by reducing ACE2. *Nature* **2023**, *615*, 134–142. [[CrossRef](#)]

20. Song, Q.Q.; Li, J.; Huo, H.X.; Cao, Y.; Wang, Y.T.; Song, Y.L.; Tu, P.F. Retention time and optimal collision energy advance structural annotation relied on LC-MS/MS: An application in metabolite identification of an antimentia agent namely echinacoside. *Anal. Chem.* **2019**, *91*, 15040–15048. [[CrossRef](#)]
21. Song, Y.L.; Song, Q.Q.; Li, J.; Zheng, J.; Li, C.; Zhang, Y.; Zhang, L.L.; Jiang, Y.; Tu, P.F. An integrated platform for directly widely-targeted quantitative analysis of feces part II: An application for steroids, eicosanoids, and porphyrins profiling. *J. Chromatogr. A* **2016**, *1460*, 74–83. [[CrossRef](#)] [[PubMed](#)]
22. Lin, M.; Chen, X.; Wang, Z.; Wang, D.; Zhang, J.L. Global profiling and identification of bile acids by multi-dimensional data mining to reveal a way of eliminating abnormal bile acids. *Anal. Chim. Acta* **2020**, *1132*, 74–82. [[CrossRef](#)] [[PubMed](#)]
23. Lan, K.; Su, M.; Xie, G.; Ferslew, B.C.; Brouwer, K.L.; Rajani, C.; Liu, C.; Jia, W. Key role for the 12-hydroxy group in the negative ion fragmentation of unconjugated C24 bile acids. *Anal. Chem.* **2016**, *88*, 7041–7048. [[CrossRef](#)] [[PubMed](#)]
24. Ma, Y.; Cao, Y.; Song, X.; Zhang, Y.; Li, J.; Wang, Y.; Wu, X.; Qi, X. BAFinder: A Software for unknown bile acid identification using accurate mass LC-MS/MS in positive and negative modes. *Anal. Chem.* **2022**, *94*, 6242–6250. [[CrossRef](#)]
25. Cao, Y.; Li, W.; Chen, W.; Niu, X.Y.; Wu, N.; Wang, Y.T.; Li, J.; Tu, P.F.; Zheng, J.; Song, Y.L. Squared energy-resolved mass spectrometry advances quantitative bile acid submetabolome characterization. *Anal. Chem.* **2022**, *94*, 15395–15404. [[CrossRef](#)]
26. Yu, Z.Q.; Yang, J.Y.; Xiang, D.; Li, G.D.; Liu, D.; Zhang, C.L. Circadian rhythms and bile acid homeostasis: A comprehensive review. *Chronobiol. Int.* **2020**, *37*, 618–628. [[CrossRef](#)]
27. Song, Y.L.; Song, Q.Q.; Liu, W.J.; Li, J.; Tu, P.F. High-confidence structural identification of metabolites relying on tandem mass spectrometry through isomeric identification: A tutorial. *Trends Analyt. Chem.* **2023**, *160*, 116982. [[CrossRef](#)]
28. Wu, Q.; Wang, J.Y.; Han, D.Q.; Yao, Z.P. Recent advances in differentiation of isomers by ion mobility mass spectrometry—ScienceDirect. *Trends Analyt. Chem.* **2020**, *124*, 115801. [[CrossRef](#)]
29. Thakare, R.; Alamoudi, J.A.; Gautam, N.; Rodrigues, A.D.; Alnouti, Y. Species differences in bile acids II. Bile acid metabolism. *J. Appl. Toxicol.* **2018**, *38*, 1336–1352. [[CrossRef](#)]
30. Deo, A.K.; Bandiera, S.M. Identification of human hepatic cytochrome p450 enzymes involved in the biotransformation of cholic and chenodeoxycholic acid. *Drug Metab. Dispos.* **2008**, *36*, 1983–1991. [[CrossRef](#)]

Disclaimer/Publisher's Note: The statements, opinions and data contained in all publications are solely those of the individual author(s) and contributor(s) and not of MDPI and/or the editor(s). MDPI and/or the editor(s) disclaim responsibility for any injury to people or property resulting from any ideas, methods, instructions or products referred to in the content.